Stress Corrosion Cracking Testing of Non-Sensitised Stainless Steel

Magnus Hansson
Seiji Yamamoto

September 2004

SKi

SKI perspective

Background

Intergranular stress corrosion cracking (IGSCC) of austenitic stainless steels has been an important concern in nuclear power plants for many years. Cracking in the heat affected zone of stainless steel piping due to chromium carbide formation at grain boundaries and chromium depletion nearby the grain boundaries (sensitisation), was an early problem for many plants. A mitigation method has been to use materials with low carbon content, i.e. Type 304L, 316L and 316 NG. These materials are considered to be less prone to sensitization because of their lower carbon content (non-sensitised materials).

In 1997, IGSCC in Type 316NG stainless steel was detected in the Forsmark nuclear power plant, Units 1 and 2. IGSCC in similar materials has also occurred elsewhere.

A literature survey on IGSCC of non-sensitised stainless steels (Jensson, Ullberg and Yamamoto, 2000), initiated by SKI, indicated that the following factors affect the IGSCC susceptibility of nuclear grade material:

- Cold work
- Crevice condition
- Austenite stability

Several researchers reported that cold worked austenitic stainless steels show susceptibility to stress corrosion cracking (SCC) even without sensitisation. Crevice conditions can enhance the corrosion, especially when combined with impurities in the environment. Austenite stability also effects IGSCC and hot cracking susceptibility. Austenitic stainless steels with high austenite stability seem to be more susceptible to IGSCC.

Purpose of the project

In this project the influence of cold work ratio and austenite stability on IGSCC has been investigated using creviced Slow Strain Rate Tests (SSRT) and Creviced Bent Beam (CBB) tests. Another aspect was to investigate if these two experimental techniques are appropriate for studying IGSCC in non-sensitised stainless steel.

Transmission Electron Microscope (TEM) studies of the test materials was also performed to investigate if any precipitations or segregations could be found at the grain boundaries which could explain the differences between the low and the high austenite stability steels.

Results

The presence of IGSCC cracks in the CBB tests shows that this method is a possible way to investigate the susceptibility of non-sensitised stainless steels to IGSCC. The creviced SSRT tests have not shown as clear results as the CBB tests.

As cold work ratio increased, both the average and the maximum crack depth increased in the CBB tests. However highly cold worked material did not show any cracks in the absence of

crevice conditions. The material with high austenite stability showed a longer maximum crack length.

TEM examinations did not reveal any precipitations or segregations in grain boundaries which could explain why the material with high austenite stability is more prone to IGSCC.

Effects on SKI work

This study is a step towards understanding the behaviour of non-sensitised stainless steels in the environment prevailing in nuclear power plants. Understanding the underlying cause of IGSCC is necessary, to be able to mitigate it and to have an effective inspection program, which is able to discover IGSCC cracks in a timely manner, in non-sensitised stainless steels.

Project information

Behnaz Aghili has been responsible for the project at SKI.
SKI reference: 14.41-021235/22226.

Stress Corrosion Cracking Testing of Non-Sensitised Stainless Steel

Magnus Hansson
Seiji Yamamoto[1]

Studsvik Nuclear AB
SE-611 82 Nyköping
Sweden

[1]Guest researcher
Toshiba Corporation
Power and Industrial Systems R&D Center

September 2004

Table of contents

Summary

Intergranular Stress Corrosion Cracking (IGSCC) in non-sensitised stainless steel has occurred in Sweden and elsewhere. The influence of cold work ratio and austenite stability, respectively, on this phenomenon has been investigated in the laboratory using creviced Slow Strain Rate Tests (SSRT) and Creviced Bent Beam (CBB) tests. A complementary aim of the study was to investigate if these two experimental techniques are appropriate for studying IGSCC in non-sensitised stainless steel.

IGSCC was obtained in the CBB tests. Most cracks initiated as transgranular cracks, but during crack propagation some of them transformed to intergranular cracks. As the cold work ratio was increased, both average and maximum crack depth increased. The maximum crack depth was considerably higher for material with high austenite stability compared to material with low austenite stability.

The CBB technique is appropriate for experimental investigations of IGSCC in non-sensitised stainless steel.

The creviced SSRT tests did not show as clear results as the CBB tests. Only transgranular cracking was obtained and any effect of the austenite stability was not observed.

The test results demonstrate that under certain conditions, such as cold work, crevice conditions, stress, and the presence of impurities, non-sensitised stainless steel exhibits transgranular cracking, which may transform into IGSCC. The effect is most significant for steels with high austenite stability, but steels with low austenite stability are also affected.

TEM studies did not show precipitations or remarkable segregation at the grain boundaries, which could explain the difference in behaviour between the low and high austenite stability steel.

Sammanfattning

Fall av interkristallin spänningskorrosion (IGSCC) har påträffats i icke-sensibiliserat rostfritt stål i kärnkraftverk i Sverige och utomlands. I denna undersökning har inverkan av kallbearbetningsgrad och austenitstabilitet på detta fenomen undersökts på laboratorium med två olika provningsmetoder, vanligen kallade *creviced SSRT* respektive *CBB*. Ett kompletterande syfte med undersökningen har varit att belysa dessa provningsmetoders användbarhet för att studera IGSCC i icke-sensibiliserat rostfritt stål.

IGSCC erhölls vid CBB-provningar. Flertalet sprickor började transkristallint, men vissa av dem omvandlades till interkristallina sprickor under propageringen. Såväl maximalt som genomsnittligt sprickdjup ökade med kallbearbetningsgraden hos materialet. Maximalt sprickdjup var väsentligt större för material med hög austenitstabilitet än för material med låg austenitstabilitet.

CBB-provning kan användas för att experimentellt undersöka IGSCC i icke-sensibiliserat rostfritt stål.

Provningen med metoden creviced SSRT gav mindre entydiga resultat än CBB-metoden. Endast transkristallin sprickinitiering erhölls och ingen inverkan av austenitstabiliteten kunde noteras.

Provningsresultaten visar att under vissa förutsättningar, som kallbearbetning, spaltmiljö, dragspänning och närvaro av föroreningar, kan transkristallina sprickor bildas i icke-sensibiliserat rostfritt stål. De transkristallina sprickorna kan övergå i IGSCC. Effekten är tydligast för material med hög austenitstabilitet, men även stål med låg austenitstabilitet påverkas.

TEM-studier påvisade varken utskiljningar eller anmärkningsvärd segring i korngränserna, som kunde förklara skillnaden i uppträdande mellan stål med låg och hög austenitstabilitet.

1 Introduction

Intergranular stress corrosion cracking (IGSCC) of austenitic stainless steel has been an important concern in nuclear power plants for many years. Cracking in the heat affected zone of stainless steel piping due to chromium depletion and chromium carbide formation at the grain boundaries was early a problem for many plants. Instead, other materials are now in use such as Type 304L, 316L and Type 316NG. These materials have lower carbon contents and are not sensitised as Type 304.

In 1997, IGSCC in Type 316NG stainless steel was detected in the Forsmark nuclear power plant, Unit 1. The position of the crack was in the heat affected zone (HAZ) located 0.3 mm from the fusion line. Measurements by EBSD showed about 22 % residual strain close to the weld, but no Cr depletion was detected on grain boundaries. The electrochemical potentiokinetic reactivation (EPR) value was very low, suggesting the material was not sensitised in a classical sense. No evidence of sensitization was revealed and there is no clear explanation for the cause of cracking.

A literature survey on IGSCC of non-sensitised stainless steels (Jenssen, Ullberg and Yamamoto, 2000), initiated by SKI, shows that the following factors affect the IGSCC susceptibility:

- Cold work
- Crevice conditions
- Austenite stability

Several researchers (Kuniya et al., 1988; Tsubota, et al., 1995; Andresen et al., 2000) reported that cold worked austenitic stainless steels show susceptibility to stress corrosion cracking (SCC) even without sensitisation. Crevice conditions can enhance the corrosion, especially when combined with impurities. But even in pure water, metal dissolution and hydrolysis can cause acidification in the crevice (Sedriks, 1996). Austenite stability, i.e. the ratio of chromium and nickel equivalents, also affects IGSCC and hot cracking susceptibility, and material with high austenite stability seems to have higher susceptibility to IGSCC (Akashi et al., 1999; Moisio et al., 1982). As a matter of fact, the austenite stability of the material used in Forsmark 1 was high, about 0.845.

In this work creviced slow strain-rate tests (SSRT) and creviced bent beam (CBB) tests were conducted for both low and high austenite stability non-sensitised cold worked Type 316NG stainless steel. Some reference samples made of sensitised as well as non-sensitised, non cold-worked Type 304 stainless steel were included. Two tests have been performed in high purity water in an autoclave at 288 °C and 9 MPa.

The aim of this work was not only to investigate the effect of cold work, crevice conditions and austenite stability on IGSCC in non-sensitised stainless steels, but also to investigate the applicability of creviced SSRT and CBB tests for examining the IGSCC susceptibility.

9

2   Experimental

2.1   Autoclave system

Testing was performed in a multi-specimen SSRT autoclave test loop. Figure 1 shows a schematic of the set-up for the experiment. At the bottom of the autoclave, 8 SSRT specimens were exposed. Above them 24 CBB test specimens, including fixtures, were placed. The volume of the autoclave was about 37 dm^3. Three thermocouples were located at different levels in the autoclave. The load of each SSRT specimen, the conductivity of the outlet water, the corrosion potential of a stainless steel working electrode and the temperature were measured and collected by a computer.
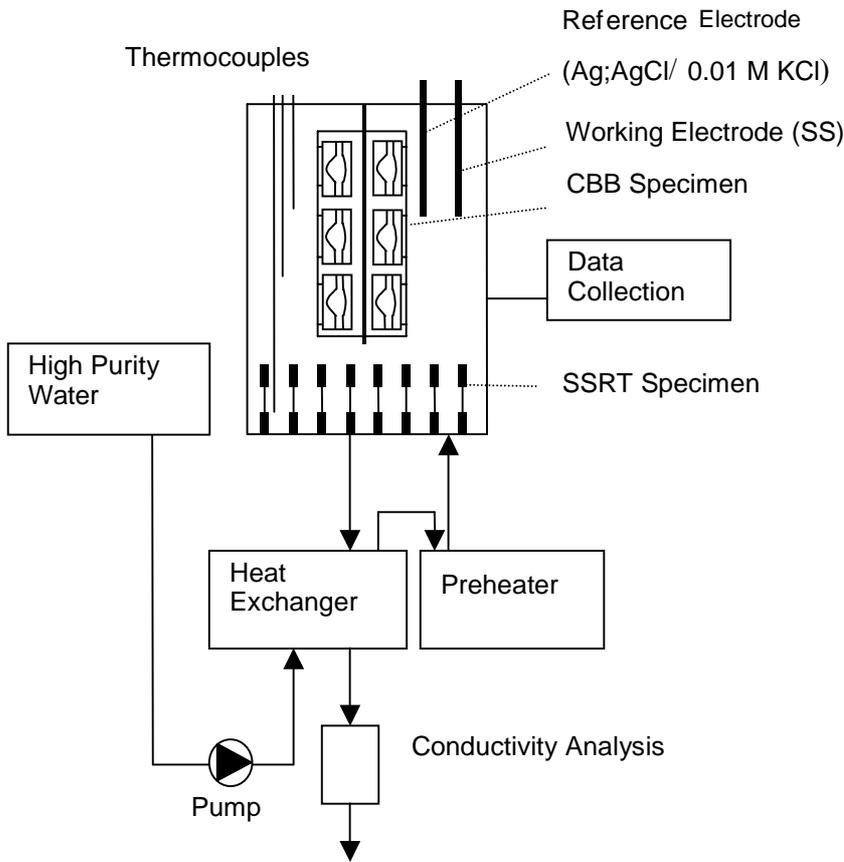

Figure 1: Experimental set-up for SSRT and CBB test.

2.2   Materials

The chemical compositions of the stainless steels used for the experiments are presented in Table 1. Type 316NG-L and Type 316NG-H are nuclear grade Type 316 steels with low and high austenite stability. Two different heats of Type 316NG-L steel have been used, one for CBB-tests called L1 and the other called L2 for SSRT-tests. The reason for this, is the thickness of the original steel material.

10

Table 1: Chemical compositions (weight percent) of the different stainless steels used

	C	Si	Mn	P	S	Cr	Ni	Mo	N	Nb
Type 316NG-L1	.019	.54	.82	.027	.006	17.6	11.2	2.06	.049	**
Type 316NG-L1*	.018	.55	.82	.030	.006	17.5	11.2	2.06	.048	.01
Type 316NG-L2*	.019	.41	1.49	.028	.001	16.4	10.5	2.57	.059	.01
Type 316NG-H	.018	.4	1.1	.017	.001	17.2	12.4	2.58	.17	**
Type 316NG-H*	.015	.43	1.15	.017	.001	17.1	12.4	2.55	.18	.01
Type 304	.040	.33	1.52	.024	.010	18.2	8.3	**	.044	**

* Check analysis
** Not measured

The austenite stability (AS) was calculated using the following equations:

$$AS = \frac{Ni-eq}{Cr-eq} \qquad \text{(Eq. 1)}$$

where: Ni-eq = [%Ni] + 30[%C] + 30[%N] + 0.5[%Mn] (Eq. 2)

Cr-eq = [%Cr] + [%Mo] + 1.5[%Si] + 0.5[%Nb] (Eq. 3)

The calculated values of the austenite stability are presented in Table 2. Values from the check analysis have been used for the Type 316 steels. The concentration of niobium was taken as zero for the Type 304.

Table 2: Austenite stability

	Austenite stability
Type 316NG-L1	0.67
Type 316NG-L2	0.69
Type 316NG-H	0.93
Type 304	0.62

Following the literature survey (Jenssen, Ullberg and Yamamoto, 2000), when AS is lower than about 0.8 the material is regarded as a material with low austenite stability. In these tests, both low and high austenite stability material were tested. According to Table 2, the two low austenite stability steels have about the same calculated value of AS.

Hardness measurements of the test materials were done using a Leitz Miniload 2. The hardness was measured using a 200 g weight on a Vickers pyramid. The materials used for the CBB tests were also examined by TEM. Details about the TEM investigations are given in Appendices E and F.

2.3 Specimens

Plates of Type 316NG were solution annealed for 30 minutes at 1050 °C and water quenched (WQ). Then the plates were cold rolled. The cold work ratio (CR) was calculated using the following equation.

$$CR = \frac{l_0 - l}{l_0} \cdot 100\%$$

(Eq. 4)

where l_0: initial thickness of the plate
       l : final thickness of the plate

Three different levels of cold work ratio were prepared. The nominal values of cold work ratio were 0 %, 7.5 % and 33 %. From these plates, cylindrical bars and rectangular plates were cut for SSRT and CBB test specimens, respectively. For both types of specimens, the rolling direction (RD) corresponds to the tensile axis.

For reference, Type 304 stainless steel specimens were also prepared. The specimens were either solution annealed or sensitised by heat-treatment for 24 hours at 620 °C in argon and furnace cooled. This corresponds to an EPR value of about 20 % (Saito et al., 2000) and the specimen is considered to be heavily sensitised. The procedure for specimen manufacturing was the same as for the Type 316NG stainless steels. Figure 2 shows the procedure for specimen preparation.
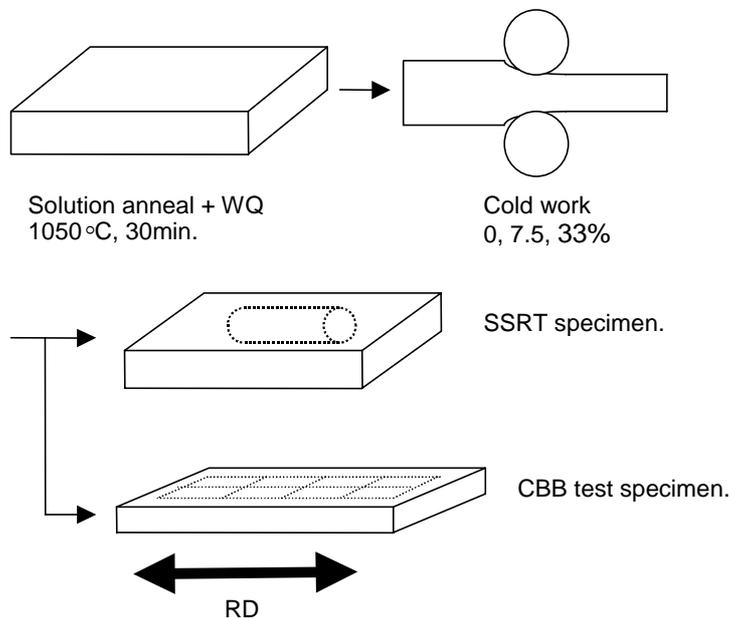

Figure 2: Procedure for specimen preparation

2.3.1 Creviced SSRT

Figure 3 shows the SSRT specimen. After cold work, $\varnothing$ 10 mm cylindrical bars were cut from the plate by electro discharge machining (EDM) and specimens were fabricated in a turning machine. The specimen surface (gauge section) was wet polished with silicon carbide (FEPA P 1000) and ultrasonically cleaned in acetone and alcohol.

To produce crevice conditions for the SSRT specimens, the gauge section of the specimen was covered with graphite fiber wool and two half-pipe metal covers, which were fixed with a Ni metal wire. In the second test covers half as long were used in order to cover a smaller part of the gauge section.
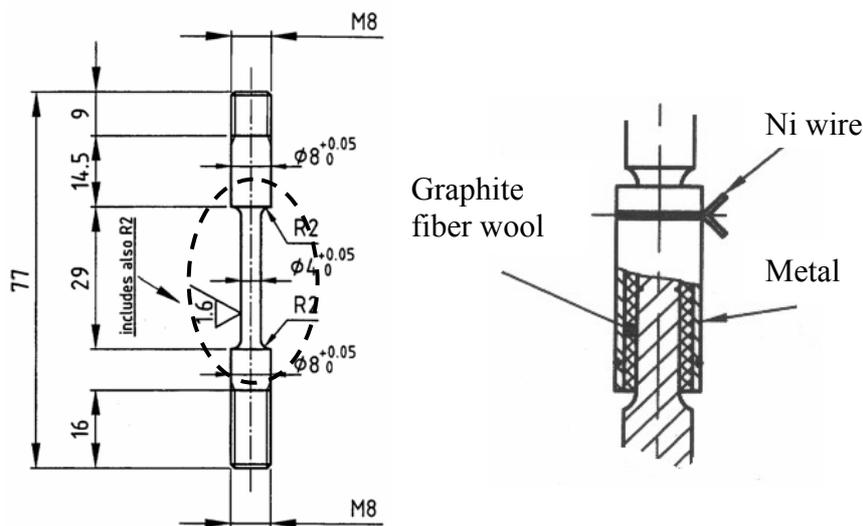

Figure 3: Dimensions of the SSRT specimen in mm.

2.3.2 CBB test

The CBB test method is described in the publications by Akashi (1988) and Akashi et al. (1979) The specimens of 316NG-L were taken from cold worked plate by water-cut, but the 316NG-H specimens were all cut out by EDM. The specimen size was a 2T × 10W × 50L (mm) rectangular plate. Before the experiments the specimen surface was wet polished with silicon carbide (FEPA P 1000) and ultrasonically cleaned in acetone and alcohol. The specimen was clamped in the holder with graphite fiber wool and two stainless steel spacers (0.2 mm thick). Figure 4 shows the CBB test specimen holder used in this experiment. The holder has two radii (100 R, 50 R) for different stress levels. Figure 5 shows the setup of CBB test specimen holders in the autoclave.
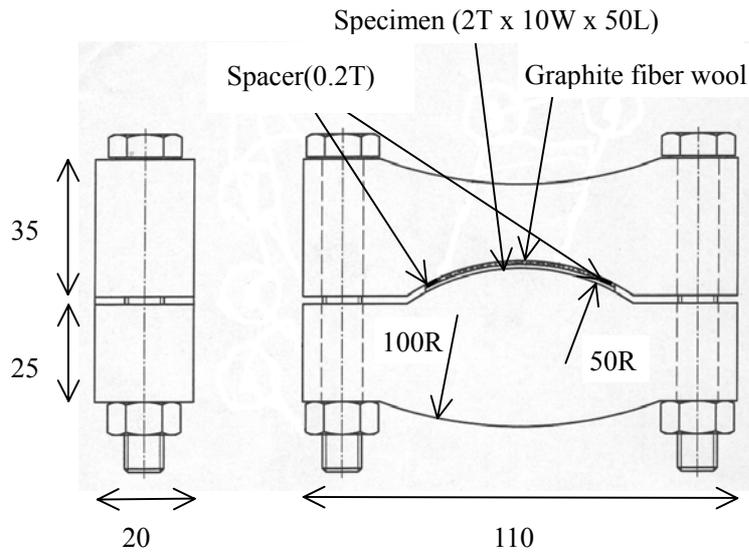
Figure 4: Dimensions of the CBB test specimen holder in mm.

2.4 Test conditions

The tests were performed in high purity water at 288 °C and 9 MPa. Before the first experiment, the graphite fiber wool and CBB specimen holders were exposed in the autoclave under the test conditions for five days to reduce the effect of any impurities in the wool and for pre-filming. Before the second test, all new screws and nuts were pre-filmed for about a week.

The flow rate of water was 18 dm^3/h in the first and 14 dm^3/h in the second test. The oxygen concentration of the inlet water was about 8 ppm. The conductivity of the inlet water was 0.06 – 0.07 µS/cm. The deviation in temperature between the thermocouples was less than 3 °C, and in the first experiment less than 1 °C.

Figure 5: Set-up of CBB test specimen holders in the autoclave.

2.4.1 Creviced SSRT

The test matrix for the first creviced SSRT is summarised in Table 3. Three cold work ratios (0, 7.5, 33 %) and two strain rates were selected for the tests. The elongation rates $1.5 \cdot 10^{-4}$ mm/min and $7.5 \cdot 10^{-4}$ mm/min were chosen in the first test. They correspond to nominal strain rates of $1 \cdot 10^{-7}$ s^{-1} and $5 \cdot 10^{-7}$ s^{-1}, respectively. As reference, a solution annealed specimen and a sensitised but not cold worked Type 304 specimens were included. In the second test, the elongation rates $7.5 \cdot 10^{-5}$ mm/min and $1.5 \cdot 10^{-4}$ mm/min were used, which correspond to strain rates $1 \cdot 10^{-7}$ s^{-1} and $5 \cdot 10^{-8}$ s^{-1}. Only Type 316NG-H and Type 316NG-L2 specimens were tested. The test matrix for the second test is summarised in Table 4.

Table 3: Test matrix for the first SSRT (Single specimens).

	Cold work ratio			Strain rate (s^{-1})	Specimen ID
	0%	7.5%	33%		
Type 316NG-L2	x			$1\cdot10^{-7}$	SA-1
		x		$1\cdot10^{-7}$	SA-2
			x	$1\cdot10^{-7}$	SA-3
	x			$5\cdot10^{-7}$	SA-4
		x		$5\cdot10^{-7}$	SA-5
			x	$5\cdot10^{-7}$	SA-6
Type 304	x			$1\cdot10^{-7}$	*SC-1
	x			$1\cdot10^{-7}$	SC-2

*SC1: Heat treatment 620 °C × 24 h in argon

Table 4: Test matrix for the second SSRT (Single specimens).

	Cold work ratio			Strain rate (s^{-1})	Specimen ID
	0%	7.5%	33%		
Type 316NG-H	x			$1\cdot10^{-7}$	SB-1
		x		$1\cdot10^{-7}$	SB-2
			x	$1\cdot10^{-7}$	SB-3
	x			$5\cdot10^{-8}$	SB-4
		x		$5\cdot10^{-8}$	SB-5
			x	$5\cdot10^{-8}$	SB-6
Type 316NG-L2		x		$5\cdot10^{-8}$	SD-1
			x	$5\cdot10^{-8}$	SD-2

2.4.2 CBB test

The test matrices of the CBB tests are summarised in Tables 5 and 6. Triplicate specimens were used for each test condition. Three cold work ratios (0, 7.5, 33 %) and two stress levels (100 R, 50 R) were selected for the experiment. If the effect of cold work is disregarded, the outer surface strain, ε, can be calculated using the following equation (Akashi, 1988):

$$\varepsilon = \frac{50 \cdot t}{R_f} \cdot \left(1 - \frac{R_f}{R_0}\right) \qquad \text{(Eq. 5)}$$

where t : the plate thickness (= 2 mm)
R_f : the final radius of the plate centre plane (= 101 or 51 mm)
R_0 : the radius of the plate before bending (= ∞)

The stress levels R=100 and R=50 correspond to strains of 1 % and 2 %, respectively. In one case (CA-6 in the first test), the specimen was clamped without graphite fiber wool to investigate the effect of the crevice former. In the first test, a solution annealed material and a sensitised but not cold worked Type 304 material was included for reference.

Table 5: Test matrix for the first set of CBB specimens (Triplicate specimens)

	Cold work ratio			Stress level		Crevice former		Specimen ID
	0%	7.5%	33%	R=100	R=50	Yes	No	
Type 316NG-L1	x			x		x		CA-1
		x		x		x		CA-2
			x	x		x		CA-3
		x			x	x		CA-4
		x			x	x		CA-5
		x			x		x	CA-6
Type 304	x			x		x		CC-1*
	x			x		x		CC-2

*) CC-1   Heat treatment 620 °C × 24 h in argon

Table 6: Test matrix for the second set CBB specimens (Triplicate specimens)

	Cold work ratio			Stress level		Crevice former		Specimen ID
	0%	7.5%	33%	R=100	R=50	Yes	No	
Type 316NG-H	x			x		x		CB-1
		x		x		x		CB-2
			x	x		x		CB-3
		x			x	x		CB-4
		x			x	x		CB-5
		x			x	x		CB-6
Type 316NG-L1				x		x		CD-1
		x				x		CD-2**
Type 304	x				x	x		CE-1*

*) CE-1   Heat treatment 620 °C × 24 h in argon
**) CD-2   Notches on the surface

3   Results

Figures A1 and A2 in Appendix A show the temperature and the outlet conductivity during the first experiment. When the autoclave was heated up to 288 °C, the outlet conductivity increased to about 2 µS/cm, and then the conductivity gradually decreased. The SSRT was started once the conductivity was lower than 0.8 µS/cm in the first test. The test period for the CBB was 650 hours. The SSRT started about 150 hours after full autoclave temperature had been reached. The second test was performed in the same way in order to keep the test times similar between the two tests. All SSRT specimens ruptured before the end of the first test, but three specimens were still unbroken when the second test ended. These three specimens were slowly pulled apart afterwards in air at room temperature.

Figures A4 and A5 in Appendix A show the temperature and the corrosion potential during the second experiment. At the beginning of the first CBB test, the potential was about 150 mV$_{SHE}$ and at the end of the test it was about 80 mV$_{SHE}$. In the second test, the corrosion potential was in the range 100 – 120 mV$_{SHE}$ during the entire test.

3.1   Creviced SSRT, first test

The loads as a function of the test time are presented in Figure A3 in Appendix A. In these curves, the pressure of the water (which corresponds to 1.1 kN) is included in the numbers shown on the y-axis. Specimen SA2 (Type 316NG-L2, 7.5 %) was not pulled correctly for about 100 hours because of problems with the pulling rod (slipping between the pullrod and the specimen holder). Specimen SA6 (Type 316NG-L2, 33 %) reached the load limit after 30 hours and was not pulled for about 40 hours. Straining of this specimen continued when this was discovered, and the load limit had been increased. The fracture surfaces of the specimens were studied in SEM (Scanning Electron Microscope). Photographs are presented in Appendix B. The results are summarised in Table 7.

3.2   Creviced SSRT, second test

In this test, only about half the gauge section of the specimens was covered with graphite wool to supress the transgranular mode of cracking, if possible. The loads as a function of test time are presented in Figure A6 in Appendix A. Due to a malfunction, specimens SB-1 and SB-6 were started about 15 hours after the other specimens. SB-3 and SB-6 reached the load limits after 140 h and 290 h, and was then not pulled correctly for about 50 h and 20 h, respectively.

Specimens SB-4, SB-5 and SB-6 did not break during the test period in the autoclave, but were slowly pulled apart afterwards in air at room temperature. In Figure A7 in Appendix A, the load as a function of test time is presented for the post-test straining. The fracture surfaces of the specimens were observed by SEM. Photographs are presented in Appendix B. The results are summarised in Table 8.

Table 7: Results of SSRT, first test.

Specimen ID	Cold work ratio (%)	Nominal strain rate (s⁻¹)	Time to failure (h)	Fracture mode ¤
SA-1	0	$1 \cdot 10^{-7}$	458	Most T
SA-2	7.5	$1 \cdot 10^{-7}$	481**	Most T
SA-3	33	$1 \cdot 10^{-7}$	224	Most D
SA-4	0	$5 \cdot 10^{-7}$	138	Most T
SA-5	7.5	$5 \cdot 10^{-7}$	122	Most T
SA-6	33	$5 \cdot 10^{-7}$	99***	Most D
SC-1*	0	$1 \cdot 10^{-7}$	157	Most I
SC-2	0	$1 \cdot 10^{-7}$	476	Mix T / D

¤   Fracture mode: D=Ductile, T=TGSCC, I=IGSCC
*   SC1: Sensitised 620°C × 24h in argon
**   SA2: Not pulled correctly for about 100 hours.
***   SA6: Not pulled correctly for about 40 hours.

Table 8: Results of SSRT, second test

Specimen ID	Cold work ratio (%)	Nominal strain rate (s⁻¹)	Time to failure (h)	Fracture mode ¤
SB-1	0	$1 \cdot 10^{-7}$	480*	Most T
SB-2	7.5	$1 \cdot 10^{-7}$	360	Most T
SB-3	33	$1 \cdot 10^{-7}$	380**	Most D
SB-4	0	$5 \cdot 10^{-8}$	¤¤	Most D
SB-5	7.5	$5 \cdot 10^{-8}$	¤¤	Most T
SB-6	33	$5 \cdot 10^{-8}$	¤¤ ***	Most D
SD-1	7.5	$5 \cdot 10^{-8}$	500	Most T
SD-2	33	$5 \cdot 10^{-8}$	510	Most D

¤   Fracture mode: D=Ductile, T=TGSCC, I=IGSCC
¤¤   SB-4, 5 and 6: Did not break during the testing in autoclave
*   SB-1: Not pulled correctly for about 15 hours.
**   SB-3: Not pulled correctly for about 50 hours.
***   SB-6: Not pulled correctly for about 35 hours.

3.3 CBB test

Subsequently to the autoclave exposure, the specimens were cut in the length direction and cross sections were polished and observed in a light optical microscope, LOM. Photographs are presented in Appendix C. Table 9 and Figures 6-7 show the results of the crack depth measurements. The second CBB test was performed in the same way, and corresponding results can be found in Table 10 and Figures 8-9. Photographs can be found in Appendix C.

Table 9: Results of the first CBB test

Specimen ID	Cold work ratio (%)	Stress level (R)	No. of cracks ≥10μm	Max. crack depth (μm)	Ave. crack depth (μm)
CA-1	0	100	0	-	-
CA-2	7.5	100	0	-	-
CA-3	33	100	5	120	100
CA-4	7.5	50	5	30	20
CA-5	33	50	10	130	60
CA-6*	33	50	0	-	--
CC-1**	0	100	10	90	30
CC-2	0	100	5	30	20

* No crevice former

** Heat treatment 620 °C × 24 h in argon
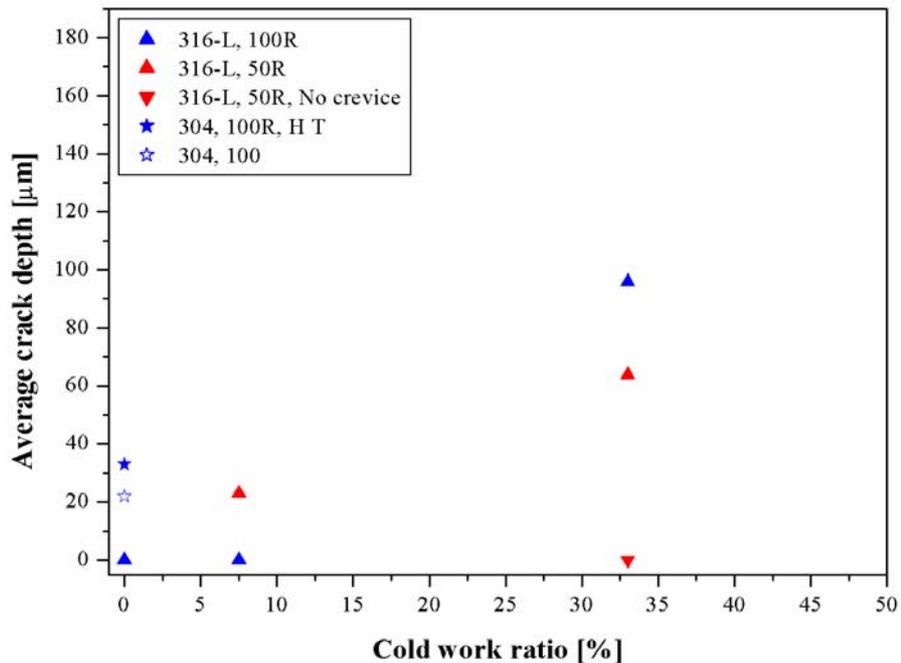
Figure 6: Average crack depth in the first CBB test
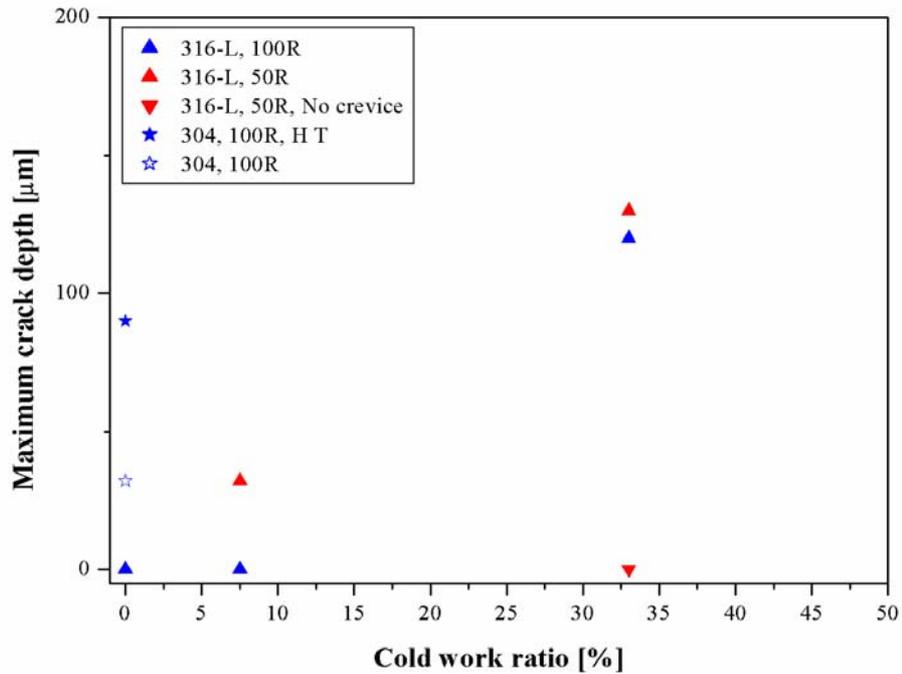
Figure 7: Maximum crack depth in the first CBB test

Table 10: Results of the second CBB test

Specimen ID	Cold work ratio (%)	Stress level (R)	No. of cracks ≥10 μm	Max. crack depth (μm)	Ave. crack depth (μm)
CB-1	0	100	170	40	20
CB-2	7.5	100	130	320	140
CB-3	33	100	90	500	170
CB-4	7.5	50	170	270	100
CB-5	33	50	100	900	190
CD-1	33	50	10	150	50
CD-2*	33	50	10	20	10
CE-1**	0	100	1¤	100¤	100¤

*   Notched specimen

**   Heat treatment 620 °C × 24 h in argon

¤   IGA, 200 μm wide at cross section
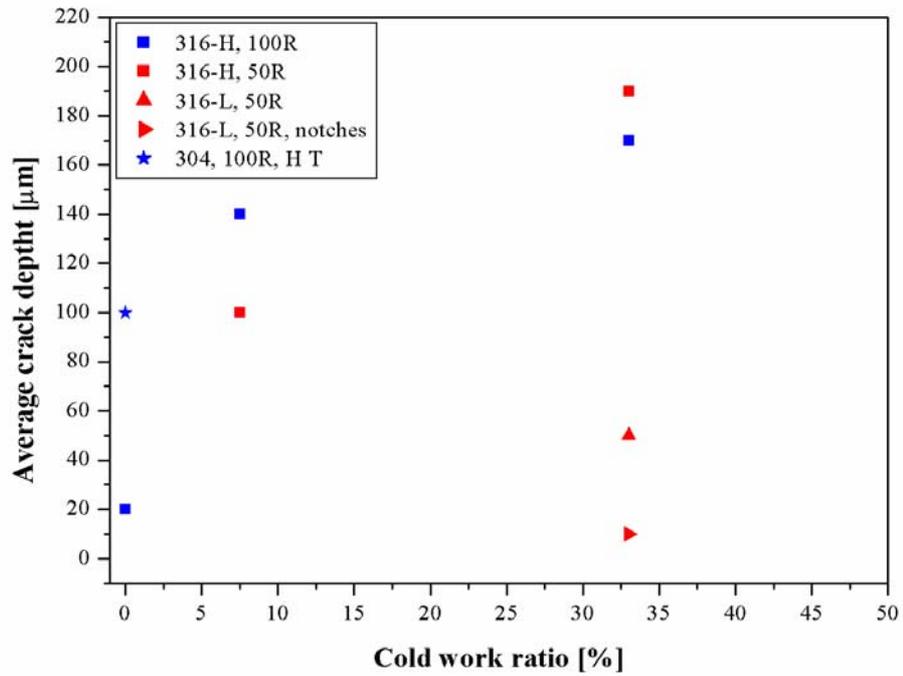
Figure 8: Average crack depth in the second CBB test
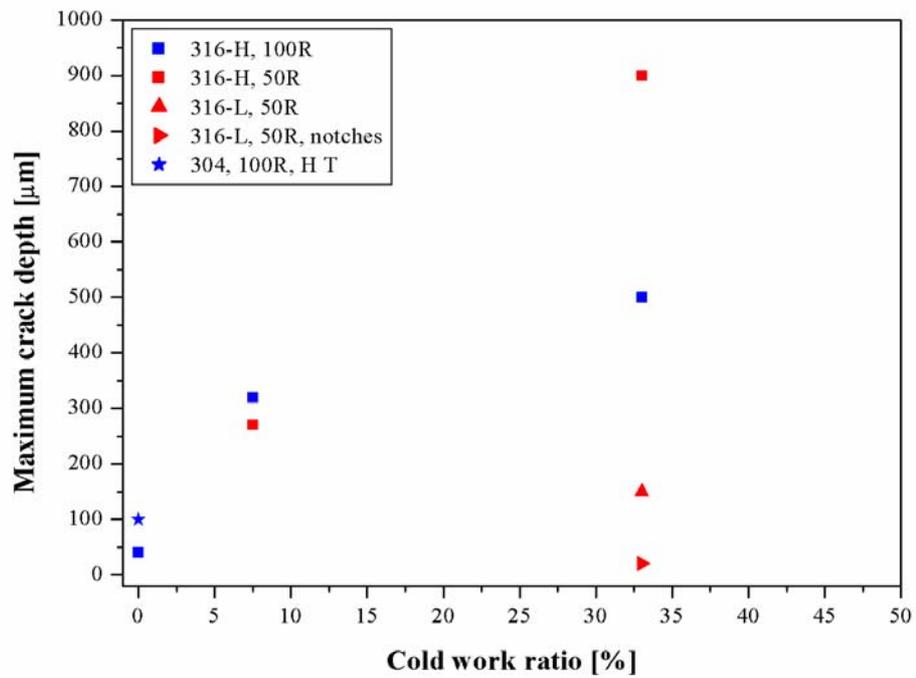
Figure 9: Maximum crack depth in the second CBB test

3.4 Hardness measurements and TEM studies

Vickers hardness measurements on cross-sections of all the original materials, from which the samples were taken, have also been done. These results are presented in Appendix D.

Four CBB samples, not tested, of low as well as high austenite stability and cold work levels of 0 % and 33 % were studied by TEM. Thin foils, about 0.15 mm, were sent to a Swedish laboratory, Nanoanalys, for further studies. Later also foils were sent to NFD, Nippon Nuclear Fuel Development Co., for additional studies. NFD volunteered for this work and their efforts are gratefully acknowledged. The TEM examinations were focused on possible differences in precipitates and grain boundary microchemistry that could explain the different behaviour of the two heats of Type 316NG. The results can be found in Appendix E and Appendix F.

4 Discussion

4.1 Effect of cold work and stress levels

In the SSRT results, cold worked materials showed, as expected, higher yield strength and they ruptured earlier than non-cold worked materials. Only sensitised 304 showed an IGSCC fracture surface, while the other materials showed only TGSCC. When the cold work ratio was 33 %, ductile fracture area was dominant. 0 % and 7.5 % cold worked materials showed similar fracture modes with a mix of ductile and TGSCC areas. The difference in the fracture mode may be related to the time to failure. In case of transgranular cracking, the crack propagation rate is proportional to the strain rate (Ford, 1979). The time to failure of SA-1 (Type 316NG-L2, 0 %) is twice as long as that for SA-3 (Type 316NG-L2, 33 %) and this is the cause of the larger TGSCC fracture area.

Two strain rates were chosen for the first experiment, but from the viewpoint of the fracture mode, there were no remarkable differences, and IGSCC fracture was not found in non-sensitised materials. It is known that the strain rate can affect the fracture mode, and a slower strain rate should be chosen for conditions where the cracking susceptibility is presumed to be low (Buzzanca et al., 1985). Therefore, a slower strain rate was chosen in the second test in order to produce IGSCC fracture, but still no IGSCC fracture occurred. Maybe the strain rate still was too high, but a lower strain rate also requires significantly longer testing times. For this reason, creviced SSRT does not seem to be a suitable testing technique for this purpose.

CBB test results showed that when the cold work ratio increased, both the average and maximum crack depth increased. In Figures 10 and 11, all average and maximum crack lengths from the two tests are put together in the same diagrams. Then it can be seen clearly that 316NG-H is more susceptible to cracking than 316NG-L. The results for those material conditions that were included in both tests do not differ in any significant way.

From the hardness measurements, Appendix D, a correlation between cold work ratio and hardness can be seen, as expected. The hardness levels were about the same for both the two low and the high austenite stability steel. As the cold work ratio increases from $0 \rightarrow 7.5 \rightarrow 33$ % the hardness of the bulk material increase from below $200 \rightarrow$ over $200 \rightarrow$ over $300 \ kg/mm^2$. In a few cases, the surface hardness is considerably higher than the bulk hardness. The samples from these materials are taken from the bulk, so this should not influence this test.

Due to different radii in the specimen holder, it was possible to investigate two stress levels in the CBB tests. No difference, between the stress levels can be seen, Figures 10 and 11. The stress levels 100R and 50R correspond to strains of 1 % and 2 %, respectively.
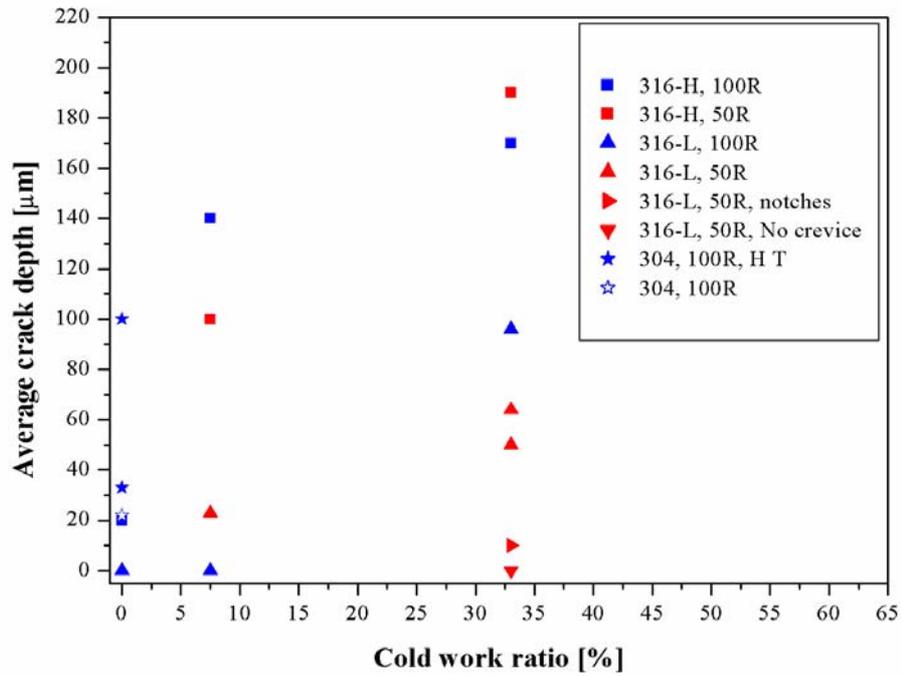
*Figure 10: Average crack depth, both CBB tests*
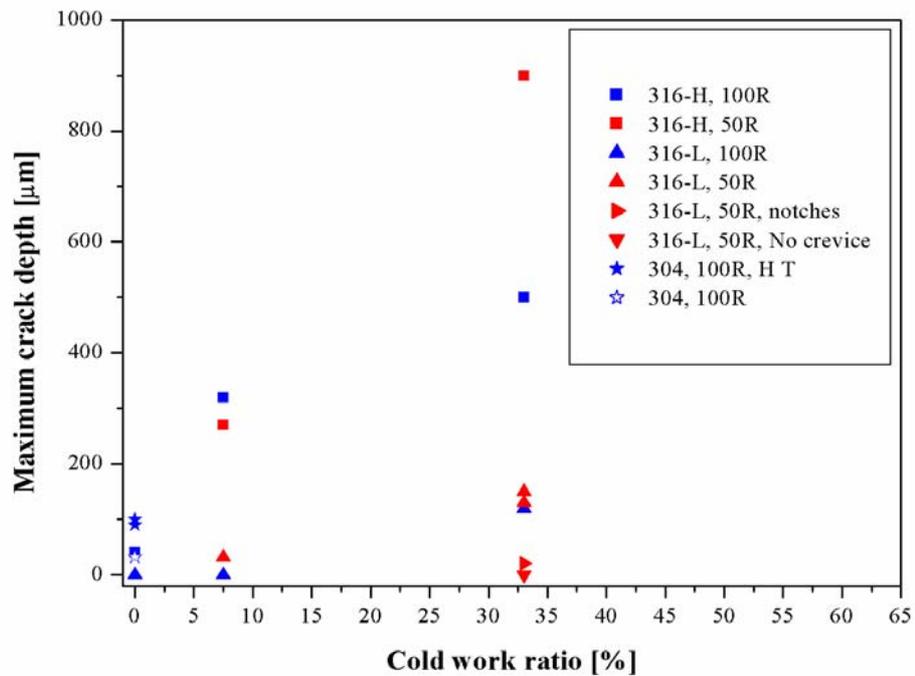
Figure 11: Maximum crack depth, both CBB tests

25

Several researchers have performed CBB tests on cold worked stainless steels. Tsubota et al. conducted CBB test on non-sensitised cold worked 316L and 304 (Tsubota, Kanazawa and Inoue, 1995). They showed that the SCC crack depth of 316L increased remarkably when the cold work ratio is higher than 30 %, see Figure 12. These cracks were TGSCC. Kuniya et al. also conducted CBB tests on non-sensitised cold worked 304 (Kuniya, Masaoka and Sasaki, 1988). Their results are similar to Tsubota's data, see Figure 13. Our results also show the same trend. However, when the crack depths are compared, the cracks in the present work are much shorter than previously reported results on both cold worked and sensitised materials. One possible explanation for the difference may be different levels of impurities in the graphite wool. The amount of graphite wool might also affect the water quality. However there is no detailed information on these issues in the published papers. The reason for the different results is therefore unclear at present.
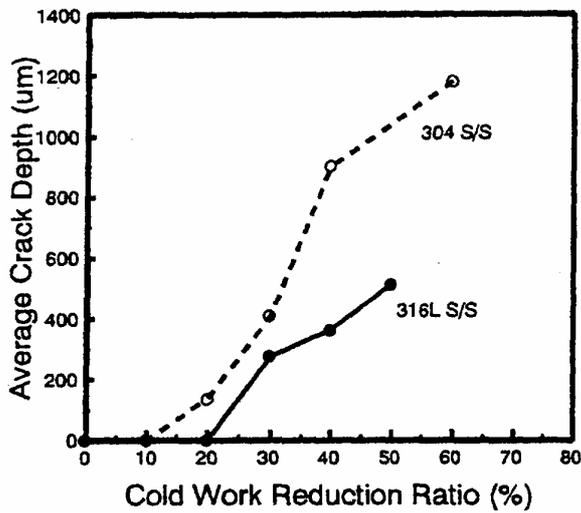

Figure 12: CBB test results in 288 °C high temperature water for cold rolled 304 S/S and 316L S/S, from Tsubota, Kanazawa and Inoue (1995).
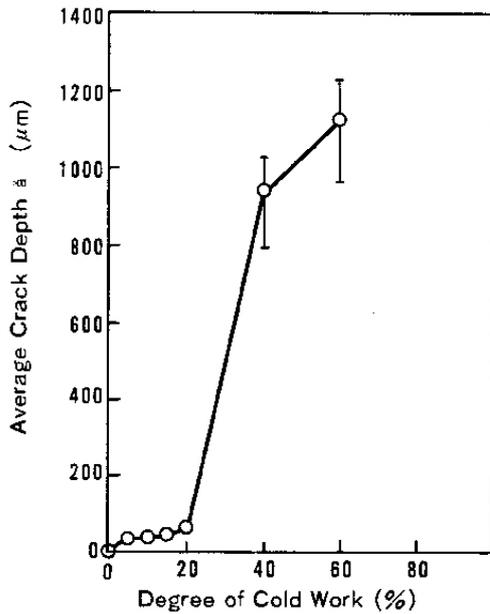
Figure 13: Average crack depth of AISI 304 SS in CBB test as a function of the degree of cold work, from Kuniya, Masaoka and Sasaki (1988).

Figure 14 shows typical cracks in cold worked CBB test specimens. In the left-hand micrograph, the crack is entirely TGSCC. In the right-hand micrograph, the crack starts as TGSCC but some branches show IGSCC. In the case of 7.5 % cold worked Type 316NG-L (CA4), the crack is not very deep but some cracks also seem to change from TGSCC to IGSCC at a certain depth. Non-cold worked Type 304 (CC2) also showed some cracks and they were all TGSCC. The number of cracks is not large and it is difficult to draw a conclusion, but during crack propagation the crack may transform from a transgranular to an intergranular mode, and cold work may somehow affect this transformation.


(a)   50μm   (b)   50μm
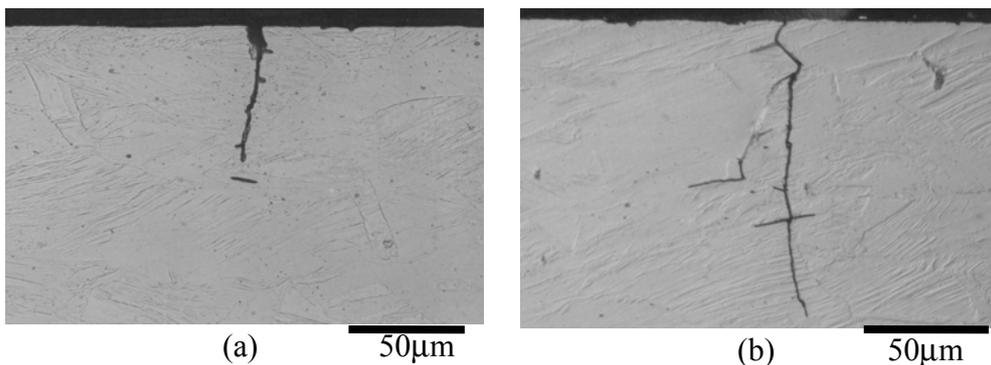
Figure 14: Cracks in the cold worked CBB test specimen Type 316NG-L1, 33 % CW

4.2 Effects of crevice and the graphite fiber wool

From CBB test results, SCC does not occur without graphite fiber wool even in the highly cold worked and highly stressed specimen (CA6).

Graphite fiber wool was used to form crevice conditions. This is a common material for CBB tests and it is known for its effectiveness in producing SCC, compared with other materials such as PTFE and stainless steels (Akashi, 1988). However the reason for this effectiveness is not clear.

In our experiments, the graphite was first washed in 288 °C air saturated water to reduce the effect of impurities. After washing there were several holes in the graphite wool, and after the experiments it was very fragile. The change in condition for the graphite wool, might result from the fact that graphite can be oxidised and dissolve in high temperature water. Figure 15 shows potential-pH diagram for the C-H_2O system at 300 °C (Chen, Aral and Theus, 1983). This figure shows that carbon is stable as HCO_3^- above the hydrogen line. It is difficult to estimate the water chemistry in the crevice, but there is a possibility that HCO_3^- existed during the experiments, and that the resultant local conductivity in the crevice was higher than that of the bulk water.

The effect of carbonate on SCC has been reported by several researchers. Indig conducted CERT (constant extension rate testing) on sensitised 304 stainless steels under BWR conditions and with several impurities such as sulfates, carbonates, nitrates and fluorides (Indig, Gordon and Davis, 1984). In his experiments carbonate was most aggressive in increasing the IGSCC. In contrast, Ljungberg showed that carbon dioxide is fairly harmless with respect to IGSCC (Ljungberg et al., 1986). His test conditions were nominally the same but the difference was the shape of the specimens. Ljungberg used notched specimens and Indig used specimens with a smooth gauge section. Ljungberg suggested that carbonate affects initiation of the crack. Our CBB test results showed no cracks without graphite wool, and this agrees with Ljungberg's idea.
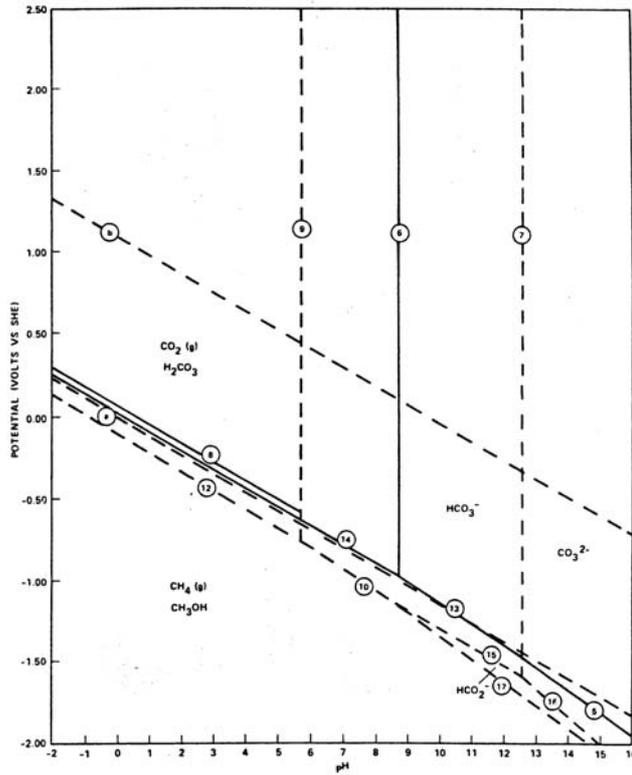
Figure 15: Potential-pH diagram for C-H₂O system at 300 °C, from Chen, Aral and Theus (1983).

4.3 Effect of other impurities

To ensure that there were no significant impurities in the graphite wool, ICP analysis of the graphite fiber wool and of the outlet water during the preparing period was conducted. The results are summarised in Tables 11 and 12.

Table 11: Results of ICP analysis of the outlet water

Element	
Ca (ppm)	<0.100
Fe (ppm)	<0.0080
K (ppm)	<0.400
Mg (ppm)	<0.0900
Na (ppm)	<0.100
S (ppm)	<0.0800
Al (ppb)	2.08 ± 0.11
As (ppb)	<1.00
Ba (ppb)	<0.200
Cd (ppb)	<0.0500
Co (ppb)	<0.0500
Cr (ppb)	2.43 ± 0.08
Cu (ppb)	<1.00
Hg (ppb)	<0.0200
Mn (ppb)	0.34 ± 0.030
Ni (ppb)	1.18 ± 0.06
Pb (ppb)	<0.2000
Zn (ppb)	3.59 ± 0.45
Cl (ppb)	<5000

Table 12: Results of ICP analysis of graphite fiber wool

Element	Washed	Not-washed
As (mg/kg)	<0.0920	<0.170
Cd (mg/kg)	0.0231 ± 0.0008	0.0577 ± 0.0012
Co (mg/kg)	1.41 ± 0.03	0.0380 ± 0.0050
Cr (mg/kg)	32.1 ± 1.0	3.08 ± 0.21
Cu (mg/kg)	4.28 ± 0.05	0.326 ± 0.009
Fe (mg/kg)	82.8 ± 2.6	17.6 ± 0.7
Hg (mg/kg)	0.0428 ± 0.0001	0.122 ± 0.001
Ni (mg/kg)	99.8 ± 3.7	2.36 ± 0.32
Pb (mg/kg)	0.713 ± 0.010	0.849 ± 0.008
S (mg/kg)	10.9 ± 1.2	92.1 ± 3.1
Zn (mg/kg)	3.21 ± 0.05	6.82 ± 0.08
Cl (mg/kg)	<500	2390 ± 130

4.4 Effect of austenite stability

As suggested in the literature survey (Jenssen, Ullberg and Yamamoto, 2000), the austenite stability affects the susceptibility of crack propagation. In Figure 10, it clearly can be seen that the average crack length is larger for the 316NG-H material, with high austenite stability. This effect is even more obvious when the maximum crack length is considered, Figure 11. In the 316NG-H material, there are some relatively long intergranular cracks, which might have started as transgranular, but transformed into IGSCC. Figure 16 shows a long IGSCC from specimen 316NG-H, 33 % cold work ratio and R = 50 (CB-5). In Appendix B, more photographs can be found.
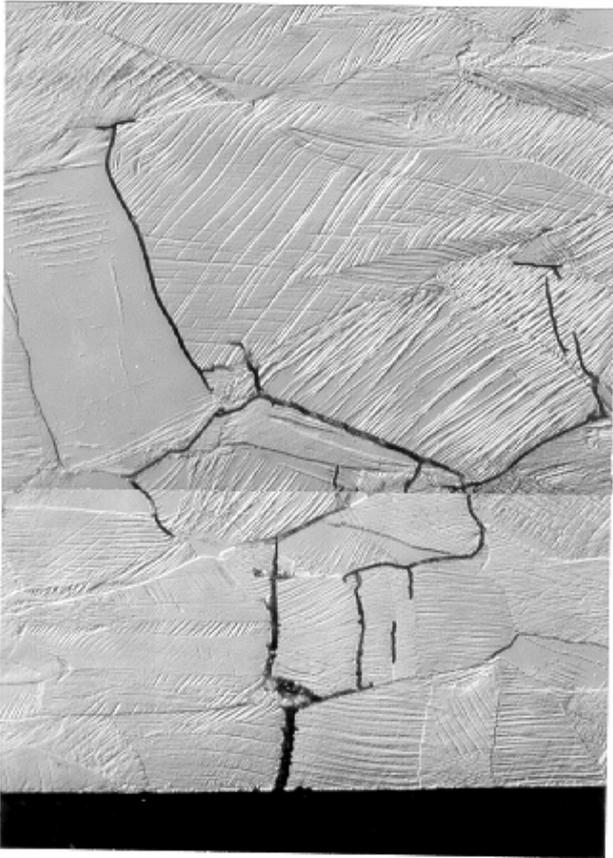
Figure 16: Specimen CB-5, Type 316NG-H, cold work ratio 33 %, 50 R. Transformation from TGSCC to IGSCC, 125 μm crack depth.

The content of nitrogen differs between the low (0.049 %) and high (0.17 %) austenite stability steel. Still no CrN was found in the grain boundaries of the H-material. As a matter of fact, no precipitates were found in the grain boundaries. In all, only very small precipitates were observed in the Type 316NG-H material. Molybdenum was enriched in the grain boundaries in the Type 316NG-L material and manganese was depleted in the Type 316NG-H. Thus, no remarkable grain boundary segregation was observed in the L or the H materials.

As pointed out in Appendix E, the density of stacking faults after deformation was higher in the material containing more N. This can be explained by the lowering of the stacking fault energy (SFE) at increasing amounts of N. The influence of the SFE may be in the way it affects the deformation of the material. In a material with low SFE, the nature of the slip would tend to be planar, as opposed to wavy in a material with high SFE. During plastic deformation, planar slip would produce well-defined and separated slip bands that can transmit dislocations into the grain boundaries. This would result in a build up of stresses at the grain boundaries and rupture the oxide film. In contrast, wavy slip produces a tangled dislocation network within the grain.

Figures 17 and 18 show two TEM photos. More TEM photos can be found in Appendices E and F.
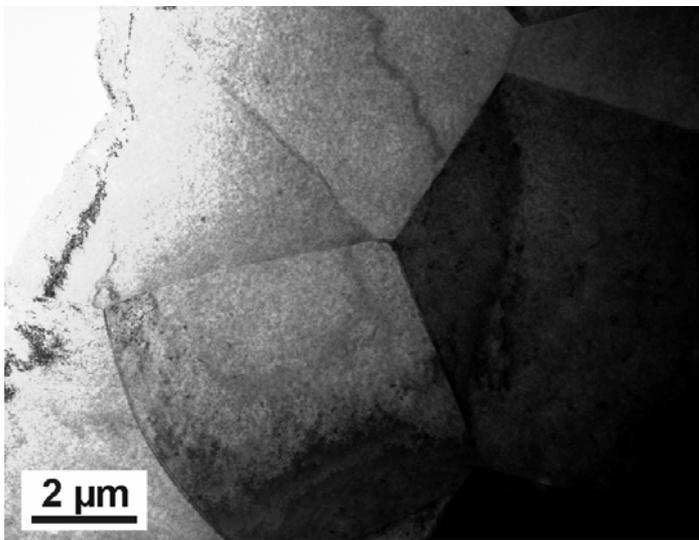
*Figure 17: Typical microstructure of Type 316NG-L1, 0 %.*
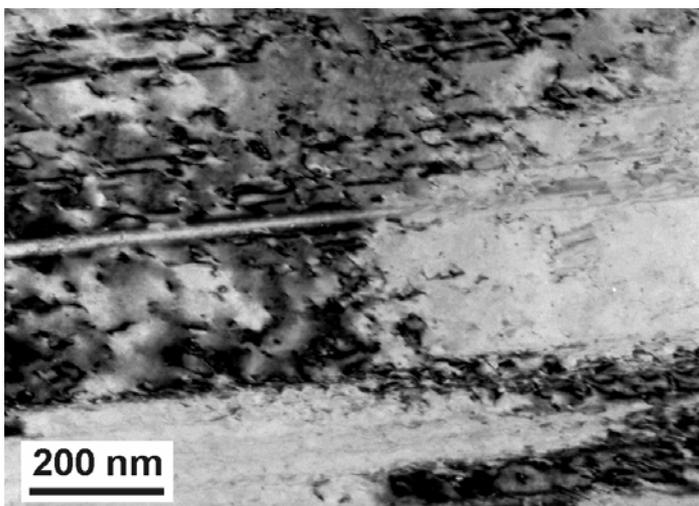
Figure 18: Twin laths in 33 % cold worked Type 316NG-H.

5   Conclusions

IGSCC susceptibility of non-sensitised stainless steels was studied by creviced SSRT and CBB tests. The presence of IGSCC cracks in the CBB tests confirms that it is a possible technique of exploring susceptibility to IGSCC of non-sensitised stainless steels. The creviced SSRT tests have not shown as clear results as the CBB tests. However, transgranular initiation was obtained.

In the creviced SSRT results, non-sensitised 316NG and 304 stainless steels showed TGSCC and ductile fracture surfaces, but no IGSCC. Only sensitised 304 showed IGSCC. No clear difference can be seen between low and high austenite stable materials with this testing technique.

From CBB test results, as the cold work ratio increased, both the average and maximum crack depths increased. However, highly cold worked material did not show any cracks in the absence of a crevice former. The maximum crack length was clearly much longer for high austenite stability material, than for material with low stability. Most cracks started as transgranular but during the crack propagation some of them transformed to intergranular cracks.

TEM examinations did not show precipitates or remarkable segregation in the grain boundaries, which could explain the difference in behaviour between the low and high austenite stability steel.

In summary, the test results show that under certain conditions such as cold work, crevice conditions, stress, and impurities, non-sensitised stainless steel shows transgranular cracking that transforms to IGSCC. This effect is most obvious for steels with high austenite stability, but also low austenite stable steels are affected.

Acknowledgements

References

Akashi, M., *CBB Test Method for Assessing the Stress Corrosion Cracking Susceptibility of Stainless Steels in High-Temperature, High-Purity Water Environments,* Elsevier Applied Science, p. 175-196 (1988).

Akashi, M. and Kawamoto, T., *Stress corrosion cracking (SCC) susceptibility of various stainless steels in oxygenated high temperature water*, IHI-Ishikawajima-Harima-Heavy-Ind.-Eng.-Rev., vol.11 (1), p. 8 (1979).

Akashi, M., Nakayama, G., Komatsu, H. and Abe, S., *Metallurgical Factors Influencing the Susceptibility of Non-Sensitized Stainless Steel to Intergranular Stress Corrosion Cracking in High-Temperature, High-Purity Water Environments*, Corrosion '99, NACE, Paper #451 (1999).

Andresen, P. L., Angeliu, T. M., Catlin, W. R., Young, L. M. and Horn, R. M. *Effect of Deformation on SCC of Unsensitized Stainless Steel,* Corrosion 2000, NACE, Paper #00203 (2000).

Buzzanca, G., Caretta, E., Meini, L., Pascali, R. and Ronchetti, C., *A contribution to the interpretation of the strain rate effect on type 304 stainless steel intergranular stress corrosion cracking*, Corrosion Science, Vol.25, No.8/9 p.805 (1985).

Chen, C. M., Aral, K. and Theus, G. J., *Computer-Calculated Potential pH Diagrams to 300°C, Volume 2: Handbook of Diagrams*, EPRI NP-3137, Volume 2, Project 1167-2, Final Report, June 1983.

Ford, P., F., *Relationship between Mechanisms of Environmental Cracking and design Criteria*, Proc. of Third Int'l Conf. On Mechanical Behavior of Materials, Vol.2, p.431 (1979).

Indig, M. E., Gordon, G. M. and Davis, R. B., *The Role of Water Purity on Stress Corrosion Cracking*, Proc. Int. Symp. Environmental Degradation of Materials in Nuclear Power Systems Water Reactors, NACE, Houston, Texas, p.506, (1984).

Jenssen, A., Ullberg, M. and Yamamoto, S., *SCC in Non-Sensitized Stainless Steel,* STUDSVIK/N-00/38, Studsvik Nuclear AB, Sweden 2000.

Kuniya, J., Masaoka, I. and Sasaki, R., *Effect of Cold Work on the Stress Corrosion Cracking of Nonsensitized AISI 304 Stainless Steel in High-Temperature Oxygenated Water*, Corrosion, Vol. 44, No.1, p. 21, (1988).

Ljungberg, L. G., Renström, K., Cubicciotti, D. and Trolle, M., *Effects of Water Impurities on Environmental Cracking in BWRs*, Proc. Second Int. Symp. Environmental Degradation of Materials in Nuclear Power Systems Water Reactors, American Nuclear Society, LaGrange Park, Illinois, p.435 (1986).

Moisio, T., Suutala, N., Kujanpää, V. and Takalo, T., *Stelning och benägenhet för varmsprickning vid svetsning av austenitiskt rostfritt stål* (in Swedish), Paper presented at Nordiska Svetsmötet (Nordic Meeting on Welding), Helsinki, Finland, June 2-4 (1982).

Saito, N., Tsuchiya, Y., Kano, F. and Tanaka, N., *Variation of Slow Strain Rate Test Fracture Mode of Type 304L Stainless Steel in 288°C Water*, Corrosion Vol.56, No.1, p.57, (2000).

Sedriks, A. J., *Corrosion of Stainless Steels*, 2nd ed., John Wiley & Sons, 1996.

Tsubota, M., Kanazawa, Y. and Inoue, H., *The Effect of Cold Work on the SCC Susceptibility of Austenitic Stainless Steels,* Proc. 7th Int. Symp. Environmental Degradation of Materials in Nuclear Power SystemsWater Reactors, NACE, Houston, TX, p.519, (1995).

www.ski.se